



Falcon: Fast Visuomotor Policies via Partial Denoising

Haojun Chen^{*1,2} Minghao Liu^{*3} Xiaojian Ma^{*2} Zailin Ma⁴ Huimin Wu² Chengdong Ma¹ Yuanpei Chen¹
Yifan Zhong¹ Mingzhi Wang¹ Qing Li² Yaodong Yang¹

Abstract

Diffusion policies are widely adopted in complex visuomotor tasks for their ability to capture multimodal action distributions. However, the multiple sampling steps required for action generation significantly harm real-time inference efficiency which limits their applicability in long-horizon tasks and real-time decision-making scenarios. Existing acceleration techniques reduce sampling steps by approximating the original denoising process but inevitably introduce unacceptable performance loss. Here we propose Falcon, which mitigates this trade-off and achieves further acceleration. The core insight is that visuomotor tasks exhibit sequential dependencies between actions at consecutive time steps. Falcon leverages this property to avoid denoising from a standard normal distribution at each decision step. Instead, it starts denoising from partial denoised actions derived from historical information to significantly reduce the denoising steps, while incorporating current observations to achieve performance-preserving acceleration of action generation. Importantly, Falcon is a training-free algorithm that can be applied as a plug-in to further improve decision efficiency on top of existing acceleration techniques. We validated Falcon in 46 simulated environments, demonstrating a 2-7x speedup with negligible performance degradation, offering a promising direction for efficient visuomotor policy design.

1. Introduction

Diffusion policies have demonstrated remarkable success in addressing complex visuomotor tasks in robotics (Chi et al.,

^{*}Equal contribution ¹Institute for Artificial Intelligence, Peking University ²National Key Laboratory of General Artificial Intelligence, BIGAI ³School of Computer Science, Peking University ⁴School of Mathematical Sciences, Peking University. Correspondence to: Qing Li <dylan.liqing@gmail.com>, Yaodong Yang <yaodong.yang@pku.edu.cn>.

2023; Reuss et al., 2023; Ze et al., 2024b;a; Ravan et al., 2024; Yang et al., 2024), thanks to their ability to model complex multimodal distributions and maintain stable training dynamics. Essentially, diffusion policies rely on the reverse sampling process of a stochastic differential equation (SDE) (Song et al., 2020b; Karras et al., 2022), where actions are iteratively sampled starting from a standard normal distribution. Each sampling step involves drawing a sample from a Brownian motion distribution, incrementally denoising the initial sample to generate the final action. However, the iterative sampling process required for action generation makes these methods computationally slow, particularly when applied to sequential decision-making in real-time environments (Chen et al., 2023b; Janner et al., 2022; Wang et al., 2022; Yang et al., 2023; Hansen-Estruch et al., 2023; Chen et al., 2023a).

To address these challenges, existing work (Song et al., 2020a;b; Lu et al., 2022; Zhang & Chen, 2022) reformulates the sampling process as an ordinary differential equation (ODE), which allows the use of numerical solvers to approximate the ODE’s solution and reduce the number of required sampling steps. However, using numerical solvers introduces inherent approximation errors, which can prevent the generation of high-quality actions in a few steps (Zhao et al., 2024). Additionally, some methods (Song et al., 2023; Kim et al., 2023; Prasad et al., 2024; Wang et al., 2024) employ distillation techniques to achieve single-step generation. While distillation improves efficiency, it compromises the ability of diffusion policies to represent multimodal action distributions, resulting in significant performance losses. Moreover, distillation-based approaches are inherently training-intensive and task-specific, meaning they cannot generalize effectively to accelerate unseen tasks or adapt to diverse visuomotor applications.

In this work, we introduce Falcon (**F**ast visuomotor policies via partial **d**enoising), a novel approach designed to bridge the gap between acceleration and performance preservation in diffusion-based visuomotor policies. The key insight behind Falcon is that sequential dependencies in visuomotor tasks can be exploited to accelerate action generation while maintaining multimodal expressiveness. To effectively leverage this property, we first utilize the previous

action prediction as the reference action, then introduce a thresholding mechanism combined with one-step estimation to evaluate which partial denoising actions are dependent on current timesteps in parallel. Using a temperature-scaled softmax, we then select the most suitable partial denoising action to continue the sampling process, preserving both performance and efficiency. By avoiding the conventional practice of starting the denoising process from a standard normal distribution at each decision step, Falcon begins from partial denoised actions derived from historical observations, significantly reducing the number of sampling steps required. Importantly, Falcon is a training-free method, which allows it to be applied as a plug-in module, enhancing the efficiency of existing diffusion-based policies without additional training or extensive modifications. It integrates seamlessly with solvers like DDIM (Song et al., 2020a) and DPMSolver (Lu et al., 2022) to further enhance acceleration.

We evaluate Falcon on various simulated environments, including RoboMimic (Mandlekar et al., 2021), RoboSuite Kitchen (Gupta et al., 2019), BlockPush (Shafiqullah et al., 2022) and MetaWorld (Yu et al., 2020). The results demonstrate that Falcon achieves a **2-7 \times** speedup in action generation with negligible performance degradation. By mitigating the trade-off between speed and performance, Falcon offers a promising direction for advancing the capabilities of diffusion policies in both simulated and real-world settings.

In summary, this work makes three main contributions: **First**, we introduce Falcon, which leverages sequential dependencies in visuomotor tasks to perform partial denoising, significantly reducing the number of sampling steps while preserving the ability to model multimodal action distributions. **Second**, Falcon functions as a training-free plug-in that enhances existing diffusion-based policies, integrating seamlessly with solvers like DDIM and DPMSolver to further accelerate action generation. **Third**, we demonstrate Falcon’s effectiveness across 46 simulated environments, achieving a **2-7 \times** speedup in inference while maintaining high action quality.

2. Preliminaries

In this section, we give a brief introduction to the diffusion model, the acceleration techniques in the diffusion model, how the diffusion models are used for diffusion policies in visuomotor tasks, and some necessary terminology.

Diffusion Models. Diffusion models, such as Denoising Diffusion Probabilistic Models (DDPM) (Ho et al., 2020), are generative models that learn data distributions by progressively corrupting data through noise in a forward process and then reconstructing it in a reverse denoising process. In the forward process, a data point \mathbf{x}_0 is corrupted K

timesteps, resulting in:

$$q(\mathbf{x}_k | \mathbf{x}_0) = \mathcal{N}(\mathbf{x}_k; \sqrt{\bar{\alpha}_k} \mathbf{x}_0, (1 - \bar{\alpha}_k) \mathbf{I}), \quad (1)$$

where $\bar{\alpha}_t = \prod_{i=1}^t \alpha_i$. After K steps, \mathbf{x}_K becomes nearly Gaussian. The reverse process reconstructs \mathbf{x}_0 by iteratively denoising, modeled as

$$p_\theta(\mathbf{x}_{k-1} | \mathbf{x}_k) = \mathcal{N}(\mathbf{x}_{k-1}; \mu_\theta(\mathbf{x}_k, k), \sigma_t^2 \mathbf{I}). \quad (2)$$

where μ_θ is the predicted mean, and σ_t^2 is fixed according to the forward process.

Accelerate techniques in the diffusion model. Some popular works (Song et al., 2020b; Karras et al., 2022; Song et al., 2020a; Lu et al., 2022) interpret the diffusion model as an ODE. Specifically, DDIM (Song et al., 2020a) generalizes the Markov forward process in DDPM to a non-Markov process, allowing the use of shorter Markov chains during sampling. The iterative steps of its sampling process can be rewritten in a form similar to Euler integration, which is a discrete solution process for a specific ODE. DPMSolver (Lu et al., 2022) accelerates sampling by analytically computing the linear part of the diffusion ODE solution and using an exponential integrator to approximate the nonlinear part. But these methods can reduce the quality degradation of few-step sampling (Shih et al., 2024).

Diffusion Policies. Diffusion policy (Chi et al., 2023) extends diffusion models as a powerful policy for visuomotor tasks. At timestep t , diffusion policy takes the latest T_o steps of observation \mathbf{O}_t as input, predicts T_p action sequence \mathbf{A}_t and executes T_a action sequence. The action sequence generation process is a conditional denoising diffusion process modeled by $p_\theta(\mathbf{A}_t | \mathbf{O}_t)$, where $\mathbf{A}_t \in \mathbb{R}^{T_p \times D_a}$ and $\mathbf{O}_t \in \mathbb{R}^{T_o \times D_o}$, D_a and D_o represent the action and observation’s dimension respectively. Specifically, starting from a pure Gaussian noise sample, diffusion policy leverage the noise prediction network ε_θ to predict and remove noise at each denoising step, iterating for K steps to generate a clean sample \mathbf{A}_t^0 . The action sequence generation process is described as equation 3, where \mathbf{A}_t^k is a partial denoising action in the timestep t with noise level k , \mathbf{Z} is a standard Gaussian random variable.

$$\mathbf{A}_t^{k-1} = \frac{1}{\sqrt{\alpha_k}} \left(\mathbf{A}_t^k - \frac{1 - \alpha_k}{\sqrt{1 - \bar{\alpha}_k}} \varepsilon_\theta(\mathbf{O}_t, \mathbf{A}_t^k, k) \right) + \sigma_k \mathbf{Z}. \quad (3)$$

The training loss is:

$$L(\theta) := \mathbb{E}_{k, \mathbf{A}_t^0, \varepsilon} \left[\left\| \varepsilon - \varepsilon_\theta(\mathbf{O}_t, \sqrt{\bar{\alpha}_k} \mathbf{A}_t^0 + \sqrt{1 - \bar{\alpha}_k} \varepsilon, k) \right\|^2 \right] \quad (4)$$

We write $[a, b]$ to denote the set $\{a, a + 1, \dots, b\}$ and $[a, b)$ to denote the set $\{a, a + 1, \dots, b - 1\}$. We write $\mathbf{x}_{a:b}$ to denote the set $\{\mathbf{x}_i : I \in [a, b)\}$ and $[K]$ to denote the set $\{1, \dots, K\}$. We define $\mathbf{A}_t = [\mathbf{a}_{t:t+T_a}, \tilde{\mathbf{a}}_{t+T_a:t+T_p}]$, where $\mathbf{a}_{t:t+T_a}$ is the executed part and $\tilde{\mathbf{a}}_{t+T_a:t+T_p}$ is the unexecuted part in timestep t .

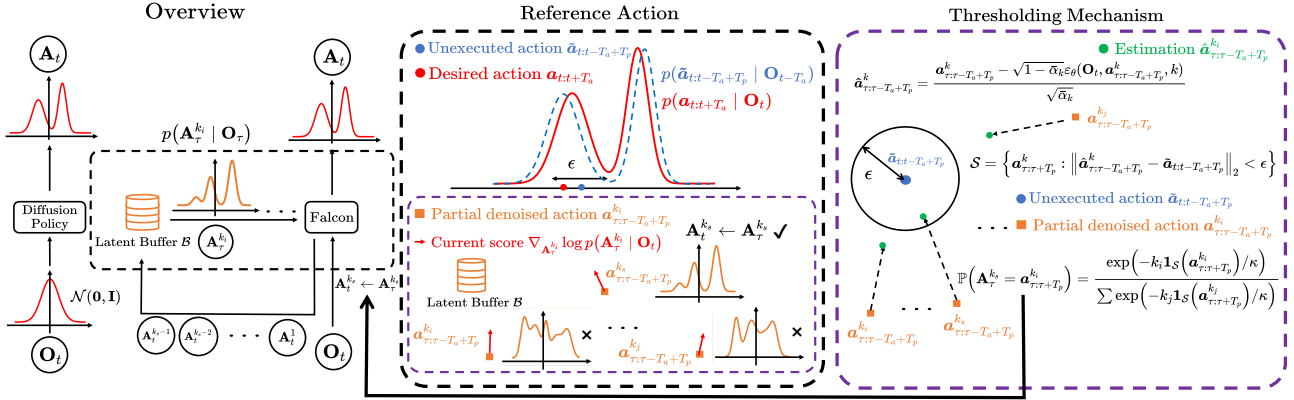


Figure 1. Method Description a) Falcon begins denoising from historically generated partial denoised actions rather than a normal distribution, requiring less than k_s steps to produce the action sequence \mathbf{A}_t . The process involves 2 steps: setting reference actions and retrieving a partial denoised action sequence $\mathbf{A}_t^{k_s}$ from the latent buffer \mathcal{B} to start denoising through a thresholding mechanism. b) Reference Action. Falcon uses unexecuted actions $\tilde{\mathbf{a}}_{t:t-T_a+T_p}$ from the previous step $t - T_a$ as the desired action $\mathbf{a}_{t:t+T_a}$, selecting a partial denoised action from \mathcal{B} as the starting point. c) Thresholding Mechanism. Falcon evaluates all actions in \mathcal{B} in parallel, identifying those close to the reference action after one-step estimation, and samples the starting point $\mathbf{A}_t^{k_s}$ based on the noise level.

3. Falcon: Fast Visuomotor Policies via Partial Denoising

In this section, we will introduce the core principles of Falcon. **First**, we present the way of leveraging previously generated action sequences $\tilde{\mathbf{a}}_{t:t-T_a+T_p}$, based on the model’s confidence in its prior predictions. **Second**, we describe the thresholding mechanism that determines which partial denoised action from past timesteps serves as the initialization for the current denoising process. **Lastly**, we outline the implementation details of Falcon.

3.1. Reference Actions

Falcon first leverages the unexecuted action sequence $\tilde{\mathbf{a}}_{t:t-T_a+T_p}$, predicted from the previous observation \mathbf{O}_{t-T_a} , as a reference for denoising the current action sequence $\mathbf{a}_{t:t+T_p}$ at time step t . This approach is motivated by our observation that the Euclidean distance $\|\tilde{\mathbf{a}}_{t:t-T_a+T_p} - \mathbf{a}_{t:t+T_p}\|_2$ between $\tilde{\mathbf{a}}_{t:t-T_a+T_p}$ and $\mathbf{a}_{t:t+T_p}$ exhibits a high probability density near zero (see Fig. 2), indicating that $\tilde{\mathbf{a}}_{t:t-T_a+T_p}$ closely approximates $\mathbf{a}_{t:t+T_p}$ in most cases.

Furthermore, as shown in Eq. 4, diffusion policies take the latest T_o observations as input and train to output the future T_p action sequence $\mathbf{A}_t = [\mathbf{a}_{t:t+T_a}, \tilde{\mathbf{a}}_{t+T_a:t+T_a+T_p}]$. This training paradigm provides confidence that the predicted action sequence $\tilde{\mathbf{a}}_{t:t-T_a+T_p} \in \mathbf{A}_t$ is sufficiently accurate for use as a reference. Additionally, Falcon incorporates the score vector field $\nabla_{\mathbf{A}_t} \log p(\mathbf{A}_t | \mathbf{O}_t)$, computed from the current observation \mathbf{O}_t , to guide the denoising process of the partial denoised action at the current time step, ensuring more precise and stable action refinement.

3.2. Thresholding Mechanism

To determine which partial denoised action from historical observations should be used as the initialization for denoising at the current timestep, we employ Tweedie’s approach (Efron, 2011; Chung et al., 2022; Kim & Ye, 2021). Given that the forward process of diffusion policy follows

$$\mathbf{A}_t^k = \sqrt{\bar{\alpha}_k} \mathbf{A}_t^0 + \sqrt{1 - \bar{\alpha}_k} \mathbf{z}, \quad \mathbf{z} \sim \mathcal{N}(\mathbf{0}, \mathbf{I}), \quad (5)$$

we derive the posterior expectation $\mathbb{E}[\mathbf{a}_{\tau:\tau-T_a+T_p}^0 | \mathbf{O}_t, \mathbf{a}_{\tau:\tau-T_a+T_p}^k]$ which serves as the one-step estimation of the partial denoised actions $\mathbf{a}_{\tau:\tau-T_a+T_p}^{k_i}$, denoted by $\hat{\mathbf{a}}_{\tau:\tau-T_a+T_p}^{k_i}$. This estimation is conditioned on the current observation \mathbf{O}_t , as formulated in Proposition 3.1. Here $\tau < t$ represents a historical decision step and k denotes the noise level of the partial denoised action $\mathbf{a}_{\tau:\tau-T_a+T_p}^k$.

The dependency between past and current actions is measured by the Euclidean distance $\|\hat{\mathbf{a}}_{\tau:\tau-T_a+T_p}^{k_i} - \tilde{\mathbf{a}}_{t:t-T_a+T_p}\|_2$ between $\hat{\mathbf{a}}_{\tau:\tau-T_a+T_p}^{k_i}$ and the reference action $\tilde{\mathbf{a}}_{t:t-T_a+T_p}$. If this distance falls below a predefined threshold ϵ , the partial denoised action $\mathbf{a}_{\tau:\tau+T_p}^k$ is selected, as it is likely to converge to the desired action $\mathbf{a}_{t:t+T_p}$.

Proposition 3.1. (Tweedie’s formula for denoising) Let \mathbf{x} be a random variable with a probability distribution $p(\mathbf{x})$, and Let $\mathbf{x}_\sigma := \mathbf{x} + \sigma \mathbf{z}$, where $\mathbf{z} \sim \mathcal{N}(0, \mathbf{I}_D)$ and $\sigma > 0$ is a known scalar. Then, the best estimate $\hat{\mathbf{x}}_\sigma$ of \mathbf{x} in mean squared error, given the noisy observation \mathbf{x}_σ , is given by the formula:

$$\hat{\mathbf{x}}_\sigma := \mathbb{E}_{p(\mathbf{x}|\mathbf{x}_\sigma)}[\mathbf{x}] = \mathbb{E}[\mathbf{x} | \mathbf{x}_\sigma] = \mathbf{x}_\sigma + \sigma^2 \nabla_{\mathbf{x}_\sigma} \log p(\mathbf{x}_\sigma) \quad (6)$$

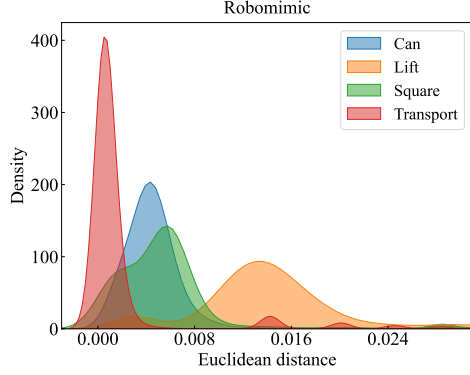


Figure 2. **Probability density estimation of $\|\tilde{\mathbf{a}}_{t:t-T_a+T_p} - \mathbf{a}_{t:t-T_a+T_p}\|_2$.** $\tilde{\mathbf{a}}_{t:t-T_a+T_p}$ is nearly the same as $\mathbf{a}_{t:t-T_a+T_p}$ since the majority of Euclidean distances between $\tilde{\mathbf{a}}_{t:t-T_a+T_p}$ and $\mathbf{a}_{t:t-T_a+T_p}$ are concentrated within the range of less than 0.015. Samples are collected by diffusion policy across four Robomimic environments (Can, Lift, Square, and Transport), where 200 trajectories were generated for each environment.

Remark 3.2. In the context of DDPM (Ho et al., 2020) whose diffusion forward process is $\mathbf{x}_t \sim \mathcal{N}(\sqrt{\bar{\alpha}_t}\mathbf{x}_0, (1 - \bar{\alpha}_t)I_D)$, Tweedie’s formula can be rewritten as

$$\mathbb{E}[\mathbf{x}_0 | \mathbf{x}_t] = (\mathbf{x}_t + (1 - \bar{\alpha}_t)\nabla_{\mathbf{x}_t} \log p(\mathbf{x}_t)) / \sqrt{\bar{\alpha}_t}. \quad (7)$$

Since $\nabla_{\mathbf{A}_t^k} \log p(\mathbf{A}_t^k | \mathbf{O}_t) = -\frac{\varepsilon}{\sqrt{1-\bar{\alpha}_k}} \approx \frac{\varepsilon_\theta(\mathbf{O}_t, \mathbf{A}_t^k, k)}{\sqrt{1-\bar{\alpha}_k}}$ (Ho et al., 2020; Chi et al., 2023), we can obtain the posterior expectation by

$$\begin{aligned} & \mathbb{E}[\mathbf{a}_{\tau:\tau-T_a+T_p}^0 | \mathbf{O}_t, \mathbf{a}_{\tau:\tau-T_a+T_p}^k] \\ &= \frac{\mathbf{a}_{\tau:\tau-T_a+T_p}^k - \sqrt{1-\bar{\alpha}_k}\varepsilon_\theta(\mathbf{O}_t, \mathbf{a}_{\tau:\tau-T_a+T_p}^k, k)}{\sqrt{\bar{\alpha}_k}} \end{aligned} \quad (8)$$

Finally, we define the set of candidate actions as $\mathcal{S} = \{\mathbf{a}_{\tau:\tau+T_p}^k : \|\hat{\mathbf{a}}_{\tau:\tau-T_a+T_p}^k - \tilde{\mathbf{a}}_{\tau:\tau-T_a+T_p}\|_2 < \epsilon, \forall \tau < t, k \in [K]\}$ and sample the starting point through the following distribution

$$\mathbb{P}\left(\mathbf{A}_\tau^{k_s} = \mathbf{a}_{\tau:\tau+T_p}^{k_i}\right) = \frac{\exp\left(-k_i \mathbf{1}_{\mathcal{S}}\left(\mathbf{a}_{\tau:\tau+T_p}^{k_i}\right) / \kappa\right)}{\sum_{\substack{\tau < t \\ k \in [K]}} \exp\left(-k_j \mathbf{1}_{\mathcal{S}}\left(\mathbf{a}_{\tau:\tau+T_p}^{k_j}\right) / \kappa\right)}, \quad (9)$$

where κ is the temperature scaling factor and $\mathbf{1}_{\mathcal{S}}(\cdot)$ is the indicator function of set \mathcal{S} . Since exclusively sampling from the latent buffer may result in idle actions, we introduce an exploration rate δ , inspired by the ϵ -greedy method from Reinforcement Learning (Sutton & Barto, 2018). With probability δ , we sample from the standard Gaussian distribution instead, ensuring more diverse behavior.

3.3. Implementation Details

In Algorithm 1, we present the pseudocode of Falcon, including threshold ϵ , exploration rate δ and latent buffer \mathcal{B} .

In practice, we can’t store all the partial denoising action generated from historical observations because of the limited GPU memory. Considering that earlier actions are generally less relevant to the current decision and that we aim to maximize efficiency, we designed a priority queue to implement the latent buffer. Partial denoising actions $\mathbf{a}_{\tau:\tau+T_p}^k$ with earlier timesteps τ and higher noise level k are given priority for removal from the queue. To prevent Falcon from repeating previous actions, we introduce k_{\min} and filter out partial denoised actions with $k < k_{\min}$ during selection. This ensures that only actions with sufficient noise levels are used in the iterative sampling process.

At timestep $t = 1$, where no prior information is available, Falcon directly samples $\mathbf{a}_{t:t+T_p}^K$ from a Gaussian distribution $\mathcal{N}(\mathbf{0}, \mathbf{I})$, and iteratively samples conditional on \mathbf{O}_t by Eq. 10 like DDPM (Ho et al., 2020) Line 7. During this process, Falcon iteratively performs denoising and stores resulting partial denoised actions $\mathbf{a}_{t:t+T_p}^k$ in a latent buffer \mathcal{B} on Line 5. This latent buffer records all partial denoised actions generated during the sampling process.

$$\begin{aligned} \mathbf{a}_{t:t+T_p}^{k-1} &= \frac{1}{\sqrt{\alpha_k}} \left(\mathbf{a}_{t:t+T_p}^k - C \right) + \sigma_k \mathbf{z}, \\ C &= \frac{1 - \alpha_k}{\sqrt{1 - \bar{\alpha}_k}} \varepsilon_\theta(\mathbf{O}_t, \mathbf{a}_{t:t+T_p}^k, k), \\ \mathbf{z} &\sim \mathcal{N}(\mathbf{0}, \mathbf{I}) \end{aligned} \quad (10)$$

For timestep $t > 1$, Falcon utilizes one-step estimation according to Eq. 8 on all stored samples $\mathbf{a}_{\tau:\tau+T_p}^{k_i}$ in the latent buffer \mathcal{B} conditioned on the current observation \mathbf{O}_t , which is the most compute-intensive part of the algorithm but can be efficiently parallelized. Line 13 obtains the partial denoising action sequence, and Line 14 sets it as the starting point of the rest of the iterative sampling process.

Falcon can also be compatible with other diffusion policy acceleration techniques by replacing the solver in Line 7 and Line 18 with other SDE/ODE solvers like DDIM (Song et al., 2020a) and DPMSolver (Lu et al., 2022). The detailed pseudocode is in the Appendix A.

4. Experiments

Our experiments aim to address three key questions: (1) Can Falcon accelerate diffusion policy, and does it further enhance speed when integrated with other acceleration algorithms (Section 4.3)? (2) Does Falcon maintain its acceleration advantage in long-sequence tasks (Section 4.4)? (3) Can Falcon retain the ability to express multimodality while achieving speed improvements (Section 4.5)?

Algorithm 1 Falcon

Require: Diffusion model ϵ_θ with noise scheduler $\bar{\alpha}_k$, variance σ_k^2 , threshold ϵ , exploration probability δ , latest T_o observations \mathbf{O}_t , latent buffer \mathcal{B} , temperature scaling factor κ .

- 1: **for** $t = 1, \dots, T$ **do**
- 2: **if** $t = 1$ **then**
- 3: $\mathbf{a}_{t:t+T_p}^K \sim \mathcal{N}(\mathbf{0}, \mathbf{I})$
- 4: **for** $k = K, \dots, 1$ **do**
- 5: $\mathcal{B} \leftarrow \mathcal{B} \cup \{\mathbf{a}_{t:t+T_p}^k\}$.
- 6: $\mathbf{z} \sim \mathcal{N}(\mathbf{0}, \mathbf{I})$ if $k > 1$, else $\mathbf{z} \leftarrow \mathbf{0}$
- 7: Sample $\mathbf{a}_{t:t+T_p}^{k-1}$ according to Eq. 10
- 8: **end for**
- 9: **end if**
- 10: **if** $t > 1$ **then**
- 11: Compute one-step estimation $\hat{\mathbf{a}}_{\tau:\tau-T_a+T_p}^{k_i}$ via Eq. 8.
- 12: $\mathcal{S} \leftarrow \{\mathbf{a}_{\tau:\tau+T_p}^k : \|\hat{\mathbf{a}}_{\tau:\tau-T_a+T_p}^{k_i} - \tilde{\mathbf{a}}_{\tau:\tau-T_a+T_p}^{k_i}\|_2 < \epsilon\}$
- 13: Sample $\mathbf{a}_{\tau:\tau+T_p}^{k_s}$ according to Eq. 9
- 14: $\mathbf{a}_{t:t+T_p}^{k_s} \leftarrow \mathbf{a}_{\tau:\tau+T_p}^{k_s}$
- 15: **for** $k = k_s, \dots, 1$ **do**
- 16: $\mathcal{B} \leftarrow \mathcal{B} \cup \{\mathbf{a}_{t:t+T_p}^k\}$.
- 17: $\mathbf{z} \sim \mathcal{N}(\mathbf{0}, \mathbf{I})$ if $k > 1$, else $\mathbf{z} \leftarrow \mathbf{0}$
- 18: Sample $\mathbf{a}_{t:t+T_p}^{k-1}$ according to Eq. 10
- 19: **end for**
- 20: **end if**
- 21: **end for**

4.1. Metrics

Our experiments are primarily evaluated by two metrics. The first is the success rate, which measures the mean and standard deviation of task completion across all trials. The second metric is generation time, quantified in terms of the Number of Function Evaluations (NFE) (Prasad et al., 2024). Since the inference cost for these models is primarily determined by NFE, and given that the network architectures are kept constant across experiments, NFE serves as a reliable indicator of relative performance. This metric effectively captures the inference cost, unbiased by GPU imbalances, and allows for a fair comparison across methods.

4.2. Simulation Environments and datasets

Robomimic (Mandlekar et al., 2021) is a large-scale benchmark designed to evaluate robotic manipulation algorithms using human demonstration datasets. Each task provides two types of human demonstrations: proficient human (PH) demonstrations, representing expert performance, and mixed proficient and nonproficient human (MH) demonstrations. Each environment uses an action prediction horizon $T_p = 16$ and an action execution horizon $T_a = 8$, and all tasks use state-based observations. We construct a CNN-based Diffusion Policy (Chi et al., 2023) with DDPM scheduler using 100 denoising steps and DDIM/DPMSolver scheduler using 16 denoising steps.

Franka Kitchen (Gupta et al., 2019) is designed for eval-

uating algorithms on long-horizon, multi-stage robotics tasks. The environment features a 9-DOF Franka robot and a kitchen scene with 7 objects for interaction and comes with a human demonstration dataset of 566 demonstrations, each completing 4 tasks in arbitrary order. The task involves action sequences of dimension 112 and an episode length of 1200, with an action prediction horizon of $T_p = 16$ and an action execution horizon of $T_a = 8$. We construct a transformer-based Diffusion Policy using a DDPM scheduler with 100-step discretization.

Multimodal Block Pushing (Shafiullah et al., 2022) tests the policy’s ability to model multimodal action distributions by pushing two blocks into two squares in any order. The demonstration data is generated by a scripted oracle with access to groundtruth state info. This oracle randomly selects an initial block to push and moves it to a randomly selected square. The remaining block is then pushed into the remaining square.

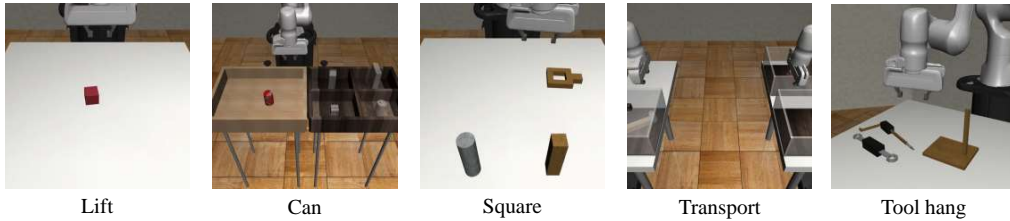
MetaWorld (Yu et al., 2020) is an open-source simulation benchmark for meta-reinforcement learning and multi-task learning. It consists of 50 different robotic manipulation tasks categorized into different difficulty levels ranging from simple to very challenging.

4.3. Falcon is a Plug & Play Acceleration Algorithm.

In the first experiment, we examine our algorithm on the robomimic benchmarks. We present the success rates, NFE, and speedup for both the original diffusion models and their Falcon-enhanced counterparts in Table 1, Table 2, and Table 3, respectively. To better understand Falcon’s impact, we categorize the tasks into simpler and more complex ones based on the level of fine-grained manipulation required. In the Robomimic benchmark (Mandlekar et al., 2021), Lift and Can are relatively simple tasks, while the remaining tasks, Square, Transport, and ToolHang, are more complex.

Simple tasks. The Lift and Can tasks involve smooth, predictable motions. In Lift, the robotic arm moves downward to grasp a small cube and then upward to lift it, with minimal variation in action within each phase. Can follows a similar pattern, where the robot picks up a coke can from a bin and places it in a target bin, primarily involving steady translational motion. Both tasks exhibit strong dependencies between consecutive actions, making them ideal for Falcon’s acceleration. As shown in Fig.5 (left), Falcon starts denoising with low noise, significantly speeding up the process. Table3 shows Falcon achieving a **7x** speedup in Lift and **2-3x** in Can, demonstrating its efficiency in structured motion tasks.

Difficult tasks. Square, Transport, and ToolHang are more complex and involve finer, more precise movements. For example, in the Transport task, two robot arms must work



	Lift		Can		Square		Transport		ToolHang
	ph	mh	ph	mh	ph	mh	ph	mh	ph
DDPM	1.00±0.00	0.95±0.07	0.98±0.13	0.97±0.15	0.91±0.07	0.85±0.35	0.80±0.39	0.65±0.47	0.52±0.49
DDPM+Falcon	1.00±0.00	0.97±0.18	0.97±0.17	0.97±0.17	0.95±0.23	0.82±0.38	0.85±0.36	0.66±0.48	0.55±0.50
DDIM	1.00±0.00	1.00±0.00	0.99±0.07	0.97±0.15	0.92±0.26	0.87±0.33	0.79±0.40	0.63±0.48	0.55±0.50
DDIM+Falcon	1.00±0.00	1.00±0.00	1.00±1.00	0.98±0.14	0.91±0.28	0.85±0.36	0.74±0.44	0.63±0.48	0.51±0.49
DPMSolver	0.98±0.12	0.95±0.20	0.97±0.21	0.97±0.17	0.93±0.25	0.84±0.36	0.70±0.45	0.55±0.49	0.58±0.49
DPMSolver+Falcon	0.98±0.14	0.96±0.20	0.96±0.20	0.98±0.14	0.94±0.24	0.90±0.30	0.74±0.43	0.54±0.50	0.56±0.48

Table 1. **Success Rate in Robomimic.** We present the success rate with 200 evaluation episodes in the format of (mean of success rate) \pm (standard deviation of success rate). Our results show that Falcon matches the original methods

together to transfer a hammer from a closed container on a shelf into a target bin on another shelf. One arm retrieves the hammer from the container, while the other arm first clears the target bin by removing trash. Then, one arm hands over the hammer to the other, which must place it in the target bin. These actions are dynamic and entail larger changes between consecutive movements. As a result, Falcon can’t start denoising actions with low noise level (see Fig. 5 (right)). Consequently, Falcon’s speedup is not as pronounced as in simpler tasks. However, even in these more challenging scenarios, as shown in Table 3, Falcon still achieves around **2x** speedup while maintaining performance close to that of the original models.

We further evaluate Falcon in MetaWorld environments using 3D Diffusion Policy (Ze et al., 2024b). The architecture follows the same setup as 3D Diffusion Policy, with a DDIM scheduler using 10-step discretization. As shown in the Appendix C, Falcon achieves a **3-4x** acceleration on top of DDIM, further demonstrating its effectiveness in accelerating existing diffusion-based policies across different tasks.

4.4. Falcon achieve acceleration diffusion policy in long horizon tasks

To evaluate Falcon’s effectiveness in long-horizon tasks, we apply it to the Franka Kitchen environment. As shown in Table 4, Falcon maintains the same high success rates as the original DDPM model, confirming that the acceleration introduced by Falcon does not compromise task performance, even for long-horizon tasks. The key benefit of Falcon lies in its ability to reduce NFE and accelerate the denoising process, which is evident in the speedup shown in Table 5. Falcon achieves a **5.25x** speedup in Kitchen, which shows

that Falcon can accelerate DDPM in long-horizon tasks and can be adopted into transformer architecture.

4.5. Falcon retains the ability to express multimodality policy

We investigate whether Falcon might compromise the ability to express multimodal policy similar to the Consistency Policy (Prasad et al., 2024). We conducted experiments in the BlockPush environment, performing 200 evaluation episodes. During these evaluations, we computed the frequency of each block being pushed to each square. Fig. 4 shows that the frequency of different policy modalities is nearly the same, indicating that Falcon does not hinder the policy’s ability to model multimodal action distributions. This uniform distribution suggests that Falcon preserves the multimodality of the diffusion policy, effectively handling different possible action combinations without bias. We also test the performance and speed in this environment. As shown in Table 4 and Table 5, Falcon achieves a **2.8x** speedup in this environment. Therefore, we conclude that Falcon maintains the ability to model multimodal policies while accelerating the denoising process, ensuring that the policy can still explore a variety of action sequences.

4.6. Ablation analysis: sensitivity to the threshold ϵ

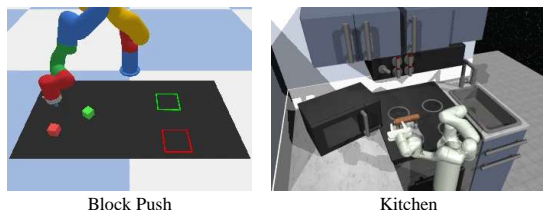
We explore how the threshold ϵ influences Falcon’s performance in the Square_ph task. The threshold ϵ determines the confidence in using partial denoised actions from previous steps to the denoising process towards the desired action \mathbf{a}_{t+T_p} guided by $\nabla_{\mathbf{A}_t^k} \log p(\mathbf{A}_t^k | \mathbf{O}_t)$. We conducted 50 evaluations using a range of ϵ values: $\{10^{-4}, 5 \times 10^{-3}, 8 \times 10^{-3}, 10^{-2}, 3 \times 10^{-2}, 5 \times 10^{-2}, 8 \times 10^{-2}, 10^{-1}\}$. As shown

	Lift		Can		Square		Transport		ToolHang
	ph	mh	ph	mh	ph	mh	ph	mh	ph
DDPM	100.0 \pm 0.0	100.0 \pm 0.0	100.0 \pm 0.0	100.0 \pm 0.0	100.0 \pm 0.0	100.0 \pm 0.0	100.0 \pm 0.0	100.0 \pm 0.0	100.0 \pm 0.0
DDPM+Falcon	12.9\pm0.3	24.6\pm1.6	35.2\pm1.3	20.3\pm0.3	37.1\pm1.5	20.5\pm0.6	46.9\pm3.7	48.0\pm4.7	33.6\pm3.2
DDIM	16.0 \pm 0.0	16.0 \pm 0.0	16.0 \pm 0.0	16.0 \pm 0.0	16.0 \pm 0.0	16.0 \pm 0.0	16.0 \pm 0.0	16.0 \pm 0.0	16.0 \pm 0.0
DDIM+Falcon	7.5\pm0.2	7.7\pm0.2	6.5\pm0.3	7.6\pm2.1	7.6\pm1.0	7.2\pm1.2	9.2\pm0.6	9.0\pm1.1	8.4\pm0.5
DPMSolver	16.0 \pm 0.0	16.0 \pm 0.0	16.0 \pm 0.0	16.0 \pm 0.0	16.0 \pm 0.0	16.0 \pm 0.0	16.0 \pm 0.0	16.0 \pm 0.0	16.0 \pm 0.0
DPMSolver+Falcon	6.4\pm0.1	10.4\pm2.0	14.7\pm0.8	10.9\pm1.8	14.4\pm0.5	7.8\pm0.9	11.0\pm1.2	12.8\pm1.4	12.1\pm1.3

Table 2. **NFE in Robomimic.** We present the NFE with 200 evaluation episodes in the format of (mean of NFE) \pm (standard deviation of NFE). Our results show that Falcon drastically reduces the denoising steps compared with the original methods

	Lift		Can		Square		Transport		ToolHang
	ph	mh	ph	mh	ph	mh	ph	mh	ph
DDPM+Falcon	7.78 \pm 0.19	4.07 \pm 0.23	2.84 \pm 0.01	4.93 \pm 0.06	2.70 \pm 0.10	4.88 \pm 0.13	2.14 \pm 0.13	2.10 \pm 0.16	2.86 \pm 0.26
DDIM+Falcon	2.13 \pm 0.03	2.08 \pm 0.06	2.45 \pm 0.11	2.15 \pm 0.24	2.15 \pm 0.22	2.27 \pm 0.32	1.71 \pm 0.10	1.88 \pm 0.18	1.92 \pm 0.09
DPMSolver+Falcon	2.48 \pm 0.02	1.60 \pm 0.32	1.09 \pm 0.07	1.51 \pm 0.25	1.11 \pm 0.04	2.09 \pm 0.21	1.48 \pm 0.17	1.27 \pm 0.13	1.32 \pm 0.12

Table 3. **Speedup in Robomimic.** We present the speed with 200 evaluation episodes in the format of (mean of speedup) \pm (standard deviation of speedup). Speed for X+Falcon is calculated by NFE of X / NFE of X+Falcon.



	BlockPush		Kitchen			
	p1	p2	p1	p2	p3	p4
DDPM	0.99	0.94	1.00	0.99	0.99	0.96
DDPM+Falcon	0.99	0.97	1.00	0.99	0.99	0.96

Table 4. **Success Rate in BlockPush and Kitchen.** For BlockPush, p_x refers to the frequency of pushing x blocks into the targets. For Kitchen, p_x refers to the frequency of interacting with x or more objects.

	BlockPush		Kitchen	
	NFE	Speedup	NFE	Speedup
DDPM	100	1.0x	100	1.0x
DDPM+Falcon	32.7	2.8x	19.03	5.25x

Table 5. **Speedup in BlockPush and Kitchen.** Falcon can accelerate diffusion policy in long-horizon tasks.

in Fig. 3 (left), when ϵ is small, Falcon is highly selective about using partial denoised actions, leading to slow denoising because Falcon frequently samples from the standard normal distribution. This results in no significant improvement. When ϵ is large, Falcon becomes overly confident in the partial denoised actions, leading to selecting many incorrect actions that do not align with \mathbf{a}_{t+T_p} , which causes a sharp drop in Score. The optimal range of ϵ lies in the middle, where Falcon can achieve speedup without sacrificing

task performance, demonstrating that a balanced ϵ allows Falcon to maintain both efficiency and accuracy.

4.7. Ablation analysis: sensitivity to exploration rate δ

We investigate how different exploration rates δ influence Falcon’s performance by running 50 evaluations across $\{0.001, 0.05, 0.0625, 0.076, 0.1, 0.2, 0.33, 1\}$ on Transport ph tasks. Exploration Rate δ controls the probability that Falcon starts the denoising process from a normal distribution rather than using the partial denoised action from the previous step. This exploration mechanism allows Falcon to fill the latent buffer with more partial denoised actions, increasing exploration and preventing over-reliance on the reference action. As shown in Fig. 3 (middle), when δ is set to 0, Falcon primarily aligns with the reference action at each step. Since the reference action is not perfectly aligned with the desired action \mathbf{A}_t , errors accumulate over time, causing Falcon to generate incorrect actions, which results in a significant drop in Score. As δ increases, the exploration rate encourages Falcon to sample more diverse actions, improving Score by reducing the accumulation of errors. However, further increasing δ results in a decrease in Speed, as the model becomes less reliant on the history of denoised actions and starts exploring more random samples from the normal distribution.

4.8. Ablation analysis: sensitivity to selection mechanism

We evaluate Falcon’s partial denoised action selection mechanism. Falcon adaptively selects partial denoised actions based on ϵ and the one-step estimation, estimating whether

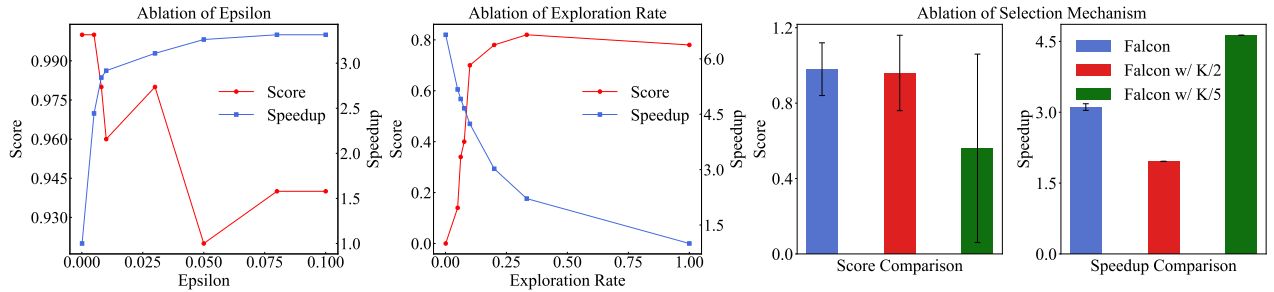


Figure 3. **Left:** Ablation analysis on threshold ϵ . The effect of varying the ϵ threshold on both the score (red circles) and speedup (blue squares), demonstrating the trade-off between performance and speed as ϵ changes. **Middle:** Ablation analysis on exploration rate δ . The score (red circles) increases sharply with δ and then stabilizes, while the speedup (blue squares) decreases as the exploration rate rises. This study highlights the balance between exploration and exploitation. **Right:** Ablation analysis on selection mechanism. This figure compares Falcon’s performance with different partial denoised action selection configurations. Restricting Falcon to choose actions with fixed noise levels ($K/2$, $K/5$) significantly reduces score, highlighting that the selection mechanism ensures accurate action choices while accelerating denoising and maintaining high performance.

each action can be denoised to A_t . We compare this with the case where Falcon is fixed to always sample from actions with noise levels of $K/2$ or $K/5$ (represented by the red and green bars), without considering the adaptive selection mechanism. Fig. 3 (right) shows a significant decrease in Score when Falcon is restricted to these fixed actions, demonstrating that not leveraging the selection mechanism compromises performance. This confirms that Falcon’s Selection Mechanism is crucial for ensuring accurate action choices, allowing the model to maintain high performance while accelerating the denoising process.

5. Related Work

Diffusion policies are widely used for modeling complex behaviors in robotics. 3D Diffusion Policy (Ze et al., 2024b) improves visuomotor performance by integrating 3D visual data from sparse point clouds. Large-scale models like Octo (Team et al., 2024) and RDT (Liu et al., 2024) scale diffusion policy parameters to build vision-language-action foundation models. However, their high computational cost limits real-time applications, necessitating acceleration techniques.

To speed up inference, sequential solvers like DDIM (Song et al., 2020a) and DPMSolver (Lu et al., 2022) reduce denoising steps, while ParaDiGMS (Shih et al., 2024) leverages parallel computing to accelerate sampling on GPUs. Distillation-based methods further improve efficiency by training models for single-step inference. Consistency Policy (Kim et al., 2023) aligns diffusion trajectories across timesteps, and ManiCM (Mu et al., 2021) extends this approach to 3D robotic tasks. OneDP (Wang et al., 2024) and SDM (Jia et al., 2024) introduce score-based distillation to reduce performance degradation. However, these methods require task-specific training, limiting adaptability. Streaming Diffusion Policy (SDP) (Høeg et al., 2024) uses partial

denoised action trajectories, similar to Falcon. However, SDP requires task-specific training and lacks compatibility with general acceleration techniques.

In contrast, Falcon is a training-free acceleration framework that leverages sequential dependencies to improve sampling speed while preserving multimodal expressiveness. It integrates seamlessly with DDIM and DPMSolver, making it a flexible, plug-and-play solution across various robotic tasks.

6. Conclusion

This paper introduces Falcon, the first diffusion policy approach to accelerate action generation in complex visuomotor tasks by leveraging inter-step dependencies in decision-making. Empirical results confirm that Falcon outperforms strong baselines, such as DDIM and DPMSolver, in terms of speed without sacrificing accuracy or expressiveness. Overall, Falcon offers a simple yet effective solution for real-time robotic tasks, providing efficient action generation for complex visuomotor environments. However, one limitation of Falcon is that it does not use a single set of parameters to accelerate all tasks, since different environments may require task-specific parameter tuning. Future work will explore adaptive parameter selection strategies to further enhance its generalizability across diverse robotic applications.

Impact Statement

Falcon removes the efficiency bottleneck of diffusion-based visuomotor policies, making real-time action generation feasible for robotic manipulation, autonomous navigation, and interactive AI. By enabling fast, high-quality decision-making in long-horizon tasks, Falcon expands the practical use of diffusion policies in real-world robot applications.

References

- Chen, H., Lu, C., Wang, Z., Su, H., and Zhu, J. Score regularized policy optimization through diffusion behavior. *arXiv preprint arXiv:2310.07297*, 2023a.
- Chen, S.-F., Wang, H.-C., Hsu, M.-H., Lai, C.-M., and Sun, S.-H. Diffusion model-augmented behavioral cloning. *arXiv preprint arXiv:2302.13335*, 2023b.
- Chi, C., Xu, Z., Feng, S., Cousineau, E., Du, Y., Burchfiel, B., Tedrake, R., and Song, S. Diffusion policy: Visuomotor policy learning via action diffusion. *The International Journal of Robotics Research*, pp. 02783649241273668, 2023.
- Chung, H., Kim, J., Mccann, M. T., Klasky, M. L., and Ye, J. C. Diffusion posterior sampling for general noisy inverse problems. *arXiv preprint arXiv:2209.14687*, 2022.
- Efron, B. Tweedie’s formula and selection bias. *Journal of the American Statistical Association*, 106(496):1602–1614, 2011.
- Gupta, A., Kumar, V., Lynch, C., Levine, S., and Hausman, K. Relay policy learning: Solving long-horizon tasks via imitation and reinforcement learning. *arXiv preprint arXiv:1910.11956*, 2019.
- Hansen-Estruch, P., Kostrikov, I., Janner, M., Kuba, J. G., and Levine, S. Idql: Implicit q-learning as an actor-critic method with diffusion policies. *arXiv preprint arXiv:2304.10573*, 2023.
- Ho, J., Jain, A., and Abbeel, P. Denoising diffusion probabilistic models. *Advances in neural information processing systems*, 33:6840–6851, 2020.
- Høeg, S. H., Du, Y., and Egeland, O. Streaming diffusion policy: Fast policy synthesis with variable noise diffusion models, 2024. URL <https://arxiv.org/abs/2406.04806>.
- Janner, M., Du, Y., Tenenbaum, J. B., and Levine, S. Planning with diffusion for flexible behavior synthesis. *arXiv preprint arXiv:2205.09991*, 2022.
- Jia, B., Ding, P., Cui, C., Sun, M., Qian, P., Fan, Z., and Wang, D. Score and distribution matching policy: Advanced accelerated visuomotor policies via matched distillation. *arXiv preprint arXiv:2412.09265*, 2024.
- Karras, T., Aittala, M., Aila, T., and Laine, S. Elucidating the design space of diffusion-based generative models. *Advances in neural information processing systems*, 35: 26565–26577, 2022.
- Kim, D., Lai, C.-H., Liao, W.-H., Murata, N., Takida, Y., Uesaka, T., He, Y., Mitsufuji, Y., and Ermon, S. Consistency trajectory models: Learning probability flow ode trajectory of diffusion. *arXiv preprint arXiv:2310.02279*, 2023.
- Kim, K. and Ye, J. C. Noise2score: tweedie’s approach to self-supervised image denoising without clean images. *Advances in Neural Information Processing Systems*, 34: 864–874, 2021.
- Liu, S., Wu, L., Li, B., Tan, H., Chen, H., Wang, Z., Xu, K., Su, H., and Zhu, J. Rdt-1b: a diffusion foundation model for bimanual manipulation. *arXiv preprint arXiv:2410.07864*, 2024.
- Lu, C., Zhou, Y., Bao, F., Chen, J., Li, C., and Zhu, J. Dpm-solver: A fast ode solver for diffusion probabilistic model sampling in around 10 steps. *Advances in Neural Information Processing Systems*, 35:5775–5787, 2022.
- Mandlekar, A., Xu, D., Wong, J., Nasiriany, S., Wang, C., Kulkarni, R., Fei-Fei, L., Savarese, S., Zhu, Y., and Martín-Martín, R. What matters in learning from offline human demonstrations for robot manipulation. *arXiv preprint arXiv:2108.03298*, 2021.
- Mu, T., Ling, Z., Xiang, F., Yang, D., Li, X., Tao, S., Huang, Z., Jia, Z., and Su, H. Maniskill: Generalizable manipulation skill benchmark with large-scale demonstrations. *arXiv preprint arXiv:2107.14483*, 2021.
- Prasad, A., Lin, K., Wu, J., Zhou, L., and Bohg, J. Consistency policy: Accelerated visuomotor policies via consistency distillation. *arXiv preprint arXiv:2405.07503*, 2024.
- Ravan, Y., Yang, Z., Chen, T., Lozano-Pérez, T., and Kaelbling, L. P. Combining planning and diffusion for mobility with unknown dynamics. *arXiv preprint arXiv:2410.06911*, 2024.
- Reuss, M., Li, M., Jia, X., and Lioutikov, R. Goal-conditioned imitation learning using score-based diffusion policies. *arXiv preprint arXiv:2304.02532*, 2023.
- Shafullah, N. M., Cui, Z., Altanzaya, A. A., and Pinto, L. Behavior transformers: Cloning k modes with one stone. *Advances in neural information processing systems*, 35: 22955–22968, 2022.
- Shih, A., Belkhale, S., Ermon, S., Sadigh, D., and Anari, N. Parallel sampling of diffusion models. *Advances in Neural Information Processing Systems*, 36, 2024.
- Song, J., Meng, C., and Ermon, S. Denoising diffusion implicit models. *arXiv preprint arXiv:2010.02502*, 2020a.

- Song, Y., Sohl-Dickstein, J., Kingma, D. P., Kumar, A., Ermon, S., and Poole, B. Score-based generative modeling through stochastic differential equations. *arXiv preprint arXiv:2011.13456*, 2020b.
- Song, Y., Dhariwal, P., Chen, M., and Sutskever, I. Consistency models. *arXiv preprint arXiv:2303.01469*, 2023.
- Sutton, R. S. and Barto, A. G. *Reinforcement learning: An introduction*. MIT press, 2018.
- Team, O. M., Ghosh, D., Walke, H., Pertsch, K., Black, K., Mees, O., Dasari, S., Hejna, J., Kreiman, T., Xu, C., et al. Octo: An open-source generalist robot policy. *arXiv preprint arXiv:2405.12213*, 2024.
- Wang, Z., Hunt, J. J., and Zhou, M. Diffusion policies as an expressive policy class for offline reinforcement learning. *arXiv preprint arXiv:2208.06193*, 2022.
- Wang, Z., Li, Z., Mandlekar, A., Xu, Z., Fan, J., Narang, Y., Fan, L., Zhu, Y., Balaji, Y., Zhou, M., et al. One-step diffusion policy: Fast visuomotor policies via diffusion distillation. *arXiv preprint arXiv:2410.21257*, 2024.
- Yang, J., Cao, Z.-a., Deng, C., Antonova, R., Song, S., and Bohg, J. Equibot: Sim (3)-equivariant diffusion policy for generalizable and data efficient learning. *arXiv preprint arXiv:2407.01479*, 2024.
- Yang, L., Huang, Z., Lei, F., Zhong, Y., Yang, Y., Fang, C., Wen, S., Zhou, B., and Lin, Z. Policy representation via diffusion probability model for reinforcement learning. *arXiv preprint arXiv:2305.13122*, 2023.
- Yu, T., Quillen, D., He, Z., Julian, R., Hausman, K., Finn, C., and Levine, S. Meta-world: A benchmark and evaluation for multi-task and meta reinforcement learning. In *Conference on robot learning*, pp. 1094–1100. PMLR, 2020.
- Ze, Y., Chen, Z., Wang, W., Chen, T., He, X., Yuan, Y., Peng, X. B., and Wu, J. Generalizable humanoid manipulation with improved 3d diffusion policies. *arXiv preprint arXiv:2410.10803*, 2024a.
- Ze, Y., Zhang, G., Zhang, K., Hu, C., Wang, M., and Xu, H. 3d diffusion policy. *arXiv preprint arXiv:2403.03954*, 2024b.
- Zhang, Q. and Chen, Y. Fast sampling of diffusion models with exponential integrator. *arXiv preprint arXiv:2204.13902*, 2022.
- Zhao, W., Bai, L., Rao, Y., Zhou, J., and Lu, J. Unipc: A unified predictor-corrector framework for fast sampling of diffusion models. *Advances in Neural Information Processing Systems*, 36, 2024.

A. Pseudocode of Falcon with other sampling solvers

In this section, we provide the pseudocode for Falcon when integrated with alternative sampling solvers, such as DDIM (Song et al., 2020a) and DPMSolver (Lu et al., 2022).

A.1. Falcon with DDIM

DDIM’s sampling process follows Eq. 11, where \mathbf{x}_k represents the sample at noise level k , α_k is the noise scheduler and ϵ_θ is the noise prediction network. To integrate Falcon with DDIM, we replace \mathbf{x}_k with partial denoised action sequence $\mathbf{a}_{t:t+T_p}^k$ at time step t with noise level k and substitute $\epsilon_\theta(\mathbf{x}_k, k)$ with $\epsilon_\theta(\mathbf{O}_t, \mathbf{a}_{t:t+T_p}^k, k)$ where \mathbf{O}_t is the latest T_o observations. This results in the modified sampling process for Falcon-enhanced diffusion policy (Eq. 12). The corresponding pseudocode is provided in Algorithm 2.

$$\mathbf{x}_{k-1} = \sqrt{\alpha_{k-1}} \left(\frac{\mathbf{x}_k - \sqrt{1 - \alpha_k} \epsilon_\theta(\mathbf{x}_k, k)}{\sqrt{\alpha_k}} \right) + \sqrt{1 - \alpha_{k-1} - \sigma_k^2} \cdot \epsilon_\theta(\mathbf{x}_k, k) + \sigma_k \epsilon_k, \quad \epsilon_k \sim \mathcal{N}(\mathbf{0}, \mathbf{I}) \quad (11)$$

$$\mathbf{a}_{t:t+T_p}^{k-1} = \sqrt{\alpha_{k-1}} \left(\frac{\mathbf{a}_{t:t+T_p}^k - \sqrt{1 - \alpha_k} \epsilon_\theta(\mathbf{O}_t, \mathbf{a}_{t:t+T_p}^k, k)}{\sqrt{\alpha_k}} \right) + \sqrt{1 - \alpha_{k-1} - \sigma_k^2} \cdot \epsilon_\theta(\mathbf{O}_t, \mathbf{a}_{t:t+T_p}^k, k) + \sigma_k \mathbf{z} \quad (12)$$

Algorithm 2 Falcon: Fast Visuomotor Policies via Partial Denoising (DDIM)

Require: Diffusion model ϵ_θ with noise scheduler $\bar{\alpha}_k$, variance σ_k^2 , threshold ϵ , exploration probability δ , latest T_o observations \mathbf{O}_t , latent buffer \mathcal{B} , $M + 1$ denoising steps $\{k_i\}_{i=0}^M$.

```

1: for  $t = 1, \dots, T$  do
2:   if  $t = 1$  then
3:      $\mathbf{a}_{t:t+T_p}^k \sim \mathcal{N}(\mathbf{0}, \mathbf{I})$ 
4:     for  $i = M, \dots, 1$  do
5:        $\mathcal{B} \leftarrow \mathcal{B} \cup \{\mathbf{a}_{t:t+T_p}^{k_i}\}$ .
6:        $\mathbf{z} \sim \mathcal{N}(\mathbf{0}, \mathbf{I})$  if  $k_i > 1$ , else  $\mathbf{z} \leftarrow \mathbf{0}$ 
7:        $\mathbf{a}_{t:t+T_p}^{k_{i-1}} \leftarrow \sqrt{\alpha_{k_{i-1}}} \left( \frac{\mathbf{a}_{t:t+T_p}^{k_i} - \sqrt{1 - \alpha_{k_i}} \epsilon_\theta(\mathbf{O}_t, \mathbf{a}_{t:t+T_p}^{k_i}, k_i)}{\sqrt{\alpha_{k_i}}} \right) + \sqrt{1 - \alpha_{k_{i-1}} - \sigma_{k_{i-1}}^2} \cdot \epsilon_\theta(\mathbf{O}_t, \mathbf{a}_{t:t+T_p}^{k_i}, k_i) + \sigma_{k_{i-1}} \mathbf{z}$ 
8:     end for
9:   end if
10:  if  $t > 1$  then
11:     $\hat{\mathbf{a}}_{\tau:\tau-T_a+T_p}^{k_i} \leftarrow \frac{1}{\sqrt{\alpha_{k_i}}} \left( \mathbf{a}_{\tau:\tau-T_a+T_p}^{k_i} - \sqrt{1 - \bar{\alpha}_{k_i}} \epsilon_\theta(\mathbf{O}_t, \mathbf{a}_{\tau:\tau-T_a+T_p}^{k_i}, k_i) \right) \quad \forall \mathbf{a}_{\tau:\tau-T_a+T_p}^{k_i} \in \mathcal{B}$ 
12:     $\mathcal{S} \leftarrow \{\mathbf{a}_{\tau:\tau+T_p}^k : \|\hat{\mathbf{a}}_{\tau:\tau-T_a+T_p}^k - \tilde{\mathbf{a}}_{\tau:\tau-T_a+T_p}^k\|_2 < \epsilon, \forall \tau < t, k \in \{k_i\}_{i=0}^M\}$ 
13:    Sample  $\mathbf{a}_{\tau:\tau+T_p}^{k_s}$  according to Eq. 9
14:     $\mathbf{a}_{t:t+T_p}^{k_s} \leftarrow \mathbf{a}_{\tau:\tau+T_p}^{k_s}$ 
15:    for  $i = s, \dots, 1$  do
16:       $\mathcal{B} \leftarrow \mathcal{B} \cup \{\mathbf{a}_{t:t+T_p}^{k_i}\}$ .
17:       $\mathbf{z} \sim \mathcal{N}(\mathbf{0}, \mathbf{I})$  if  $k_i > 1$ , else  $\mathbf{z} \leftarrow \mathbf{0}$ 
18:       $\mathbf{a}_{t:t+T_p}^{k_{i-1}} \leftarrow \sqrt{\alpha_{k_{i-1}}} \left( \frac{\mathbf{a}_{t:t+T_p}^{k_i} - \sqrt{1 - \alpha_{k_i}} \epsilon_\theta(\mathbf{O}_t, \mathbf{a}_{t:t+T_p}^{k_i}, k_i)}{\sqrt{\alpha_{k_i}}} \right) + \sqrt{1 - \alpha_{k_{i-1}} - \sigma_{k_{i-1}}^2} \cdot \epsilon_\theta(\mathbf{O}_t, \mathbf{a}_{t:t+T_p}^{k_i}, k_i) + \sigma_{k_{i-1}} \mathbf{z}$ 
19:    end for
20:  end if
21: end for

```

A.2. Falcon with DPMSolver

Given a noise prediction network ϵ_θ , denoising steps $\{k_i\}_{i=0}^M$, DPMSolver’s sampling process follows Eq. 13, where $h_{i-1} = \log \frac{\alpha_{k_{i-1}}}{\sigma_{k_{i-1}}} - \log \frac{\alpha_{k_i}}{\sigma_{k_i}}$. To integrate Falcon, we replace \mathbf{x}_{k_i} with $\mathbf{a}_{t:t+T_p}^{k_i}$ and substitute $\epsilon_\theta(\mathbf{x}_{k_i}, k_i)$ with $\epsilon_\theta(\mathbf{O}_t, \mathbf{a}_{t:t+T_p}^{k_i}, k_i)$, where \mathbf{O}_t represents the latest T_o observations. This yields the sampling process in diffusion policy with DPMSolver, as expressed in Eq. 14. The corresponding pseudocode is provided in Algorithm 3.

$$\mathbf{x}_{k_{i-1}} = \frac{\alpha_{k_{i-1}}}{\alpha_{k_i}} \mathbf{x}_{k_i} - \sigma_{k_{i-1}} (e^{h_{i-1}} - 1) \epsilon_\theta(\mathbf{x}_{k_i}, k_i) \quad (13)$$

$$\mathbf{a}_{t:t+T_p}^{k_{i-1}} = \frac{\alpha_{k_{i-1}}}{\alpha_{k_i}} \mathbf{a}_{t:t+T_p}^{k_i} - \sigma_{k_{i-1}} (e^{h_{i-1}} - 1) \epsilon_\theta(\mathbf{O}_t, \mathbf{a}_{t:t+T_p}^{k_i}, k_i) \quad (14)$$

Algorithm 3 Falcon: Fast Visuomotor Policies via Partial Denoising (DPMSolver)

Require: Diffusion model ϵ_θ with noise scheduler $\bar{\alpha}_k$, variance σ_k^2 , threshold ϵ , exploration probability δ , latest T_o observations \mathbf{O}_t , latent buffer \mathcal{B} and $M + 1$ denoising steps $\{k_i\}_{i=0}^M$.

```

1: for  $t = 1, \dots, T$  do
2:   if  $t = 1$  then
3:      $\mathbf{a}_{t:t+T_p}^K \sim \mathcal{N}(\mathbf{0}, \mathbf{I})$ 
4:      $\mathbf{a}_{t:t+T_p}^M \leftarrow \mathbf{a}_{t:t+T_p}^K$ 
5:     for  $i = M, \dots, 1$  do
6:        $\mathcal{B} \leftarrow \mathcal{B} \cup \{\mathbf{a}_{t:t+T_p}^{k_i}\}$ .
7:        $h_{i-1} \leftarrow \log \frac{\alpha_{k_{i-1}}}{\sigma_{k_{i-1}}} - \log \frac{\alpha_{k_i}}{\sigma_{k_i}}$ 
8:        $\mathbf{a}_{t:t+T_p}^{k_{i-1}} = \frac{\alpha_{k_{i-1}}}{\alpha_{k_i}} \mathbf{a}_{t:t+T_p}^{k_i} - \sigma_{k_{i-1}} (e^{h_{i-1}} - 1) \epsilon_\theta(\mathbf{O}_t, \mathbf{a}_{t:t+T_p}^{k_i}, k_i)$ 
9:     end for
10:  end if
11:  if  $t > 1$  then
12:     $\hat{\mathbf{a}}_{\tau:\tau-T_a+T_p}^{k_i} \leftarrow \frac{1}{\sqrt{\alpha_{k_i}}} \left( \mathbf{a}_{\tau:\tau-T_a+T_p}^{k_i} - \sqrt{1 - \bar{\alpha}_{k_i}} \epsilon_\theta(\mathbf{O}_t, \mathbf{a}_{\tau:\tau-T_a+T_p}^{k_i}, k_i) \right) \quad \forall \mathbf{a}_{\tau:\tau-T_a+T_p}^{k_i} \in \mathcal{B}$ 
13:     $\mathcal{S} \leftarrow \{\mathbf{a}_{\tau:\tau+T_p}^k : \|\hat{\mathbf{a}}_{\tau:\tau-T_a+T_p}^{k_i} - \hat{\mathbf{a}}_{\tau:\tau-T_a+T_p}^k\|_2 < \epsilon, \forall \tau < t\}$ 
14:    Sample  $\mathbf{a}_{\tau:\tau+T_p}^{k_s} \sim P(\mathbf{a}_{\tau:\tau+T_p}^{k_s}) = \frac{\exp k_s}{\sum \exp k_i}$  in  $\mathcal{S}$ 
15:     $\mathbf{a}_{t:t+T_p}^{k_s} \leftarrow \mathbf{a}_{\tau:\tau+T_p}^{k_s}$ 
16:    for  $i = s, \dots, 1$  do
17:       $\mathcal{B} \leftarrow \mathcal{B} \cup \{\mathbf{a}_{t:t+T_p}^{k_i}\}$ .
18:       $h_{i-1} \leftarrow \log \frac{\alpha_{k_{i-1}}}{\sigma_{k_{i-1}}} - \log \frac{\alpha_{k_i}}{\sigma_{k_i}}$ 
19:       $\mathbf{a}_{t:t+T_p}^{k_{i-1}} = \frac{\alpha_{k_{i-1}}}{\alpha_{k_i}} \mathbf{a}_{t:t+T_p}^{k_i} - \sigma_{k_{i-1}} (e^{h_{i-1}} - 1) \epsilon_\theta(\mathbf{O}_t, \mathbf{a}_{t:t+T_p}^{k_i}, k_i)$ 
20:    end for
21:  end if
22: end for

```

B. Visualization of Multimodality

In this section, we provide a visualization of the multimodal action distributions generated by Falcon in the BlockPush environment. As shown in Fig. 4, the frequency distribution of different action modalities in the BlockPush task, where each modality corresponds to a distinct combination of blocks being pushed into two squares. The chart illustrates the uniformity of the action modality frequencies, with the four modalities (1-2, 1-1, 2-1, and 2-2) being equally represented. This visualization confirms that Falcon is capable of expressing multimodal actions, effectively handling different action combinations without bias.

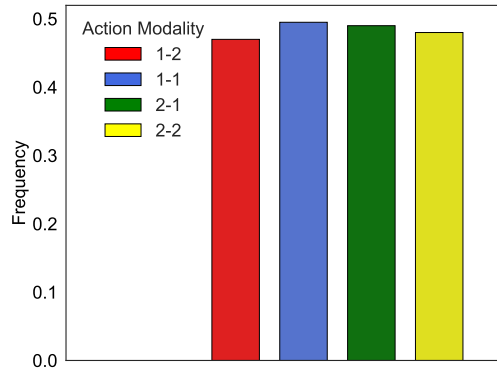


Figure 4. Action Modalities Distribution in BlockPush Task. The bar chart shows the frequency of different policy modalities for pushing two blocks into two squares in any order. The modalities are represented as 1-2, 1-1, 2-1, and 2-2, where the numbers indicate the block number and square number respectively. The chart illustrates the frequency distribution of the action modalities generated by Falcon in the BlockPush task.

C. Detail performance of Falcon with 3D Diffusion Policy

In this section, we provide a detailed results of Falcon’s acceleration performance when applied to 3D Diffusion Policy (Ze et al., 2024b) in MetaWorld environments. Falcon is integrated with DDIM using 10-step discretization (we call 3D FalconDDIM), following the original 3D Diffusion Policy architecture to ensure a fair comparison.

Tables 6, 7 and 8 present the success rates, NFE and speedup respectively, for both 3D Diffusion Policy and 3D FalconDDIM. These results further validate Falcon’s effectiveness in reducing inference time while maintaining task performance across different robotic manipulation tasks.

Table 6. Detailed results for 39 simulated tasks with success rates. We evaluated 39 challenging tasks using 50 random seeds and reported the average success rate (%) and standard deviation for each task individually. The 3D FalconDDIM algorithm demonstrates nearly no performance drop.

Alg \ Task	Meta-World (Easy)					
	Button Press	Coffee Button	Plate Slide Back Side	Plate Slide Side	Window Close	Window Open
3D Diffusion Policy	100 ± 0	100 ± 0	100 ± 0	100 ± 0	100 ± 0	100 ± 0
3D FalconDDIM	100 ± 0	100 ± 0	100 ± 0	100 ± 0	100 ± 0	100 ± 0

Alg \ Task	Meta-World (Easy)					
	Button Press Topdown	Button Press Topdown Wall	Button Press Wall	Peg Unplug Side	Door Close	Door Lock
3D Diffusion Policy	100 ± 0	99 ± 2	99 ± 1	75 ± 5	100 ± 0	98 ± 2
3D FalconDDIM	100 ± 0	100 ± 0	100 ± 0	75 ± 43	100 ± 0	96 ± 19

Alg \ Task	Meta-World (Easy)						
	Door Open	Door Unlock	Drawer Close	Drawer Open	Faucet Close	Faucet Open	Handle Press
3D Diffusion Policy	99 ± 1	100 ± 0	100 ± 0	100 ± 0	100 ± 0	100 ± 0	100 ± 0
3D FalconDDIM	100 ± 0	100 ± 0	100 ± 0	100 ± 0	100 ± 0	100 ± 0	100 ± 0

Alg \ Task	Meta-World (Easy)					
	Handle Pull Side	Lever Pull	Plate Slide	Plate Slide Back	Dial Turn	Reach
3D Diffusion Policy	85 ± 3	79 ± 8	100 ± 1	99 ± 0	92 ± 27	68 ± 46
3D FalconDDIM	87 ± 33	81 ± 39	86 ± 34	100 ± 0	89 ± 31	68 ± 46

Alg \ Task	Meta-World (Medium)						Meta-World (Hard)	
	Hammer	Basketball	Push Wall	Box Close	Sweep	Sweep Into	Assembly	Hand Insert
3D Diffusion Policy	88 ± 32	98 ± 2	88 ± 32	56 ± 49	96 ± 3	15 ± 5	99 ± 1	12 ± 32
3D FalconDDIM	83 ± 37	100 ± 0	88 ± 32	55 ± 49	100 ± 0	13 ± 33	99 ± 9	26 ± 43

Alg \ Task	Meta-World (Hard)	Meta-World (Very Hard)				
	Push	Shelf Place	Disassemble	Stick Pull	Stick Push	Pick Place Wall
3D Diffusion Policy	51 ± 3	52 ± 49	72 ± 44	68 ± 46	97 ± 4	80 ± 40
3D FalconDDIM	53 ± 49	47 ± 49	75 ± 43	68 ± 46	100 ± 0	87 ± 33

Fast Visuomotor Policies via Partial Denoising

Table 7. Detailed results for 39 simulated tasks with NFE. We evaluated 39 challenging tasks using 50 random seeds and reported the average Number of Function Evaluations (nfe) per action generation and standard deviation for each domain individually. The 3D FalconDDIM algorithm reduces the nfe to a range of 2-4 compared to the 3D Diffusion Policy

		Meta-World (Easy)					
Alg \ Task	Button Press	Coffee Button	Plate Slide Back Side	Plate Slide Side	Window Close	Window Open	
3D Diffusion Policy	10 ± 0	10 ± 0	10 ± 0	10 ± 0	10 ± 0	10 ± 0	
3D FalconDDIM	2.12 ± 0.05	2.47 ± 0.09	3.91 ± 0.22	3.27 ± 0.68	2.54 ± 0.18	3.58 ± 0.90	

		Meta-World (Easy)					
Alg \ Task	Button Press Topdown	Button Press Topdown Wall	Button Press Wall	Peg Unplug Side	Door Close	Door Lock	
3D Diffusion Policy	10 ± 0	10 ± 0	10 ± 0	10 ± 0	10 ± 0	10 ± 0	
3D FalconDDIM	2.48 ± 0.20	2.63 ± 0.40	3.36 ± 0.61	3.25 ± 0.38	2.81 ± 0.05	4.06 ± 1.00	

		Meta-World (Easy)					
Alg \ Task	Door Open	Door Unlock	Drawer Close	Drawer Open	Faucet Close	Faucet Open	Handle Press
3D Diffusion Policy	10 ± 0	10 ± 0	10 ± 0	10 ± 0	10 ± 0	10 ± 0	10 ± 0
3D FalconDDIM	3.04 ± 0.26	4.70 ± 0.86	2.91 ± 0.47	3.90 ± 0.18	4.06 ± 0.62	4.94 ± 0.78	3.52 ± 0.43

		Meta-World (Easy)					
Alg \ Task	Handle Pull Side	Lever Pull	Plate Slide	Plate Slide Back	Dial Turn	Reach	
3D Diffusion Policy	10 ± 0	10 ± 0	10 ± 0	10 ± 0	10 ± 0	10 ± 0	
3D FalconDDIM	3.59 ± 0.51	3.79 ± 0.77	3.11 ± 0.15	3.49 ± 0.16	4.26 ± 1.16	2.85 ± 0.05	

		Meta-World (Medium)					Meta-World (Hard)	
Alg \ Task	Hammer	Basketball	Push Wall	Box Close	Sweep	Sweep Into	Assembly	Hand Insert
3D Diffusion Policy	10 ± 0	10 ± 0	10 ± 0	10 ± 0	10 ± 0	10 ± 0	10 ± 0	10 ± 0
3D FalconDDIM	3.25 ± 0.60	2.97 ± 0.14	3.35 ± 0.22	4.51 ± 1.12	3.09 ± 0.18	3.59 ± 0.19	2.44 ± 0.23	3.29 ± 0.19

		Meta-World (Hard)	Meta-World (Very Hard)				
Alg \ Task	Push	Shelf Place	Disassemble	Stick Pull	Stick Push	Pick Place Wall	
3D Diffusion Policy	10 ± 0	10 ± 0	10 ± 0	10 ± 0	10 ± 0	10 ± 0	
3D FalconDDIM	2.88 ± 0.38	4.28 ± 2.33	3.25 ± 0.37	3.78 ± 0.73	3.41 ± 0.32	3.04 ± 0.15	

Fast Visuomotor Policies via Partial Denoising

Table 8. Detailed results for 39 simulated tasks with speedup. We evaluated 39 challenging tasks using 50 random seeds and reported the average speedup and standard deviation for each task individually. The 3D FalconDDIM algorithm reduces the NFE to a range of 2-4 compared to the 3D Diffusion Policy

		Meta-World (Easy)							
Alg \ Task		Button Press	Coffee Button	Plate Slide Back Side	Plate Slide Side	Window Close	Window Open		
3D FalconDDIM		4.71 ± 0.12	4.03 ± 0.14	2.55 ± 0.14	3.05 ± 0.60	3.93 ± 0.28	2.79 ± 0.66		
		Meta-World (Easy)							
Alg \ Task		Button Press Topdown	Button Press Topdown Wall	Button Press Wall	Peg Unplug Side	Door Close	Door Lock		
3D FalconDDIM		4.02 ± 0.32	3.80 ± 0.48	2.97 ± 0.47	3.07 ± 0.34	3.55 ± 0.06	2.46 ± 0.51		
		Meta-World (Easy)							
Alg \ Task		Door Open	Door Unlock	Drawer Close	Drawer Open	Faucet Close	Faucet Open	Handle Press	
3D FalconDDIM		3.28 ± 0.26	2.12 ± 0.32	3.42 ± 0.36	2.55 ± 0.12	2.45 ± 0.35	2.02 ± 0.35	2.83 ± 0.30	
		Meta-World (Easy)							
Alg \ Task		Handle Pull Side	Lever Pull	Plate Slide	Plate Slide Back	Dial Turn	Reach		
3D FalconDDIM		2.77 ± 0.36	2.63 ± 0.44	3.21 ± 0.15	2.86 ± 0.14	2.34 ± 0.56	3.50 ± 0.06		
		Meta-World (Medium)					Meta-World (Hard)		
Alg \ Task		Hammer	Basketball	Push Wall	Box Close	Sweep	Sweep Into	Assembly	Hand Insert
3D FalconDDIM		3.25 ± 0.60	2.97 ± 0.14	3.35 ± 0.22	4.51 ± 1.12	3.09 ± 0.18	3.59 ± 0.19	2.44 ± 0.23	3.29 ± 0.19
		Meta-World (Hard)	Meta-World (Very Hard)						
Alg \ Task		Push	Shelf Place	Disassemble	Stick Pull	Stick Push	Pick Place Wall		
3D FalconDDIM		2.88 ± 0.38	2.33 ± 0.65	3.07 ± 0.30	2.64 ± 0.44	2.92 ± 0.25	3.28 ± 0.14		

D. Experiment Details

In this section, we provide the detailed experimental setup for Robomimic and analyze Falcon’s memory cost compared to the original samplers (DDPM, DDIM, and DPMSolver). Table 9 reports the hyperparameter settings and the peak memory usage for each experiment.

To evaluate Falcon’s computational overhead, we measure the peak memory cost, denoted in the format (original sampler cost) + (incremental cost due to Falcon integration). As shown in Table 9, Falcon introduces an additional 12 MB of memory overhead, which is negligible compared to the original 1876 MB cost. This demonstrates that Falcon achieves acceleration with minimal memory overhead, making it a practical and efficient enhancement to diffusion-based policies.

	DDPM+Falcon					DDIM+Falcon					DPMSolver+Falcon				
	ϵ	δ	k_{\min}	$ \mathcal{B} $	Peak Memory Cost	ϵ	δ	k_{\min}	$ \mathcal{B} $	Peak Memory Cost	ϵ	δ	k_{\min}	$ \mathcal{B} $	Peak Memory Cost
Lift ph	0.04	0.1	20	50	1876+12 MB	0.05	0.2	15	50	1876+12 MB	0.08	0.2	20	50	1876+12 MB
Lift mh	0.04	0.1	20	50	1876+12 MB	0.03	0.25	10	50	1876+12 MB	0.005	0.2	20	50	1876+12 MB
Can ph	0.01	0.1	20	50	1876+12 MB	0.01	0.20	8	50	1876+12 MB	0.003	0.2	20	50	1876+12 MB
Can mh	0.01	0.1	20	50	1876+12 MB	0.005	0.20	8	50	1876+12 MB	0.003	0.2	20	50	1876+12 MB
Square ph	0.04	0.1	25	50	1876+12 MB	0.01	0.20	8	50	1876+12 MB	0.003	0.2	25	20	1876+12 MB
Square mh	0.04	0.1	25	50	1876+12 MB	0.005	0.20	3	50	1876+12 MB	0.005	0.2	20	20	1876+12 MB
Transport ph	0.01	0.2	25	50	1876+12 MB	0.005	0.33	8	50	1876+12 MB	0.005	0.2	20	20	1876+12 MB
Transport mh	0.01	0.2	25	50	1876+12 MB	0.01	0.33	5	50	1876+12 MB	0.003	0.2	60	50	1876+12 MB
ToolHang ph	0.01	0.1	20	50	1876+12 MB	0.01	0.33	5	50	1876+12 MB	0.003	0.2	60	50	1876+12 MB

Table 9. Hyperparameters and Memory Cost in Robomimic.

E. Visualization of Starting Points

This section visualizes where Falcon starts the denoising process at each time step, specifically from which past time step and at what noise level the partial denoised actions originate. We analyze two tasks: Lift ph and Transport ph, representing high and low acceleration scenarios, respectively.

As shown in Fig.5 (left), in the Lift task, Falcon consistently starts denoising from the partial denoised action of the previous time step, with a low noise level. This indicates a significant reduction in sampling steps, leading to substantial acceleration. In contrast, Fig.5 (right) shows that the Transport task starts from actions with higher noise levels, limiting the acceleration effect. This suggests that Falcon’s speedup is more pronounced in tasks with smoother, more predictable action transitions.

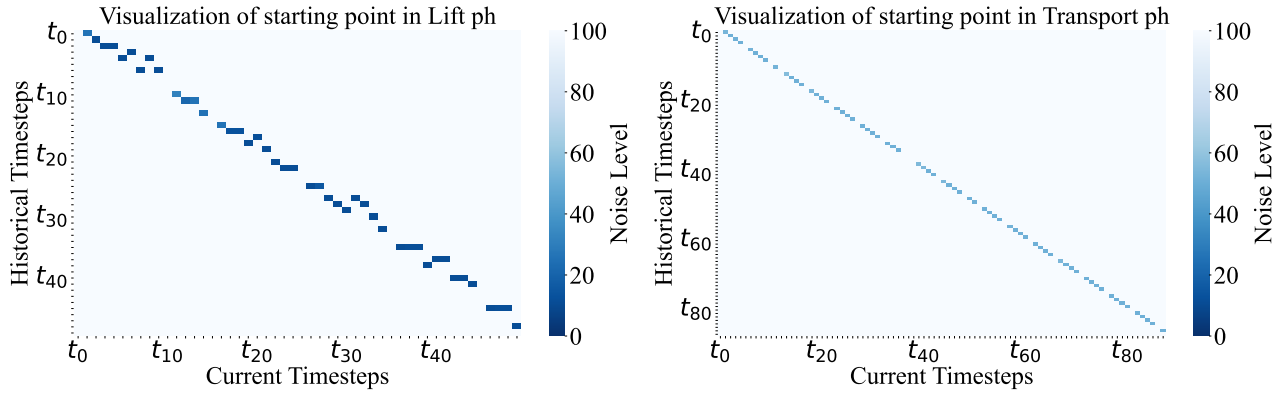


Figure 5. **Visualization of denoising starting point.** This figure shows the heatmaps $A \in \mathbb{R}^{T \times T}$ in Lift ph task (left) and Transport ph task (right). $A[j, i] = k$ means that at time step i , Falcon starts denoising at the partial denoised actions $\mathbf{a}_{l:j+T_p}^k$.